ELSEVIER

Current Applied Physics 1 (2001) 45–49

Current Applied Physics
Physics, Chemistry and Materials Science

www.elsevier.com/locate/cap

Far-infrared to visible optical conductivity of single-wall carbon nanotubes

A. Ugawa, J. Hwang, H.H. Gommans, H. Tashiro, A.G. Rinzler, D.B. Tanner *

Department of Physics, University of Florida, 215 Williamson, Gainesville, FL 32611-8440, USA

Received 28 August 2000; accepted 8 September 2000

Abstract

The reflectance of unoriented single-wall carbon nanotube films has been measured over a wide wavelength range (far-IR–UV). The results are consistent with the film being a mixture of conducting (armchair), small bandgap ($n \equiv m$, mod 3) and semiconducting nanotubes. The optical conductivity shows peaks corresponding to transitions between density-of-states peaks of these tubes, at energy locations consistent with 1.4 nm diameter tubes. In addition optical absorption spectroscopy of aligned single-wall carbon nanotubes shows that the optical transitions are well-aligned along the tube axis. This behavior is consistent with polarized resonant Raman and electronic structure calculations.

PACS: 78.30.Na; 71.20.Tx; 78.20.Ci
Keywords: Nanotubes; Infrared; Fullerenes

Carbon nanotubes have been very widely studied ever since their discovery [1] on account of their unique electronic [2–4] and mechanical [5,6] properties, properties that vary with the symmetry and environment of the tubes. Several workers have investigated the electronic structures of isolated single-wall nanotubes (SWNT) as well as bundled nanoropes. For isolated tubes it is believed that (n,n) (armchair) SWNT are metallic, whereas $(n,0)$ (zigzag) and (n,m) (chiral) tubes are semiconducting, most with a gap of 0.7 eV or so [2,3,7]. In certain cases ($n \equiv m$, mod 3), tube curvature is predicted to induce a very small bandgap [2,7]. It has also been theorized that nanoropes made from (n,n) nanotubes develop a pseudogap due to a broken symmetry caused by intertube coupling [8]. This paper describes some results of far-infrared–ultraviolet optical spectroscopy of SWNT, prepared as free-standing films.

Laser-vaporization grown SWNT [9] were purified, made into free-standing films, and characterized as described in Ref. [10]. The films had thickness of typically 20–40 μm. They were opaque over the entire wavelength range studied. The reflectance was measured on a Bruker IFS 113v using a reflectance unit and a liquid Helium flow cryostat. The sample is rigidly affixed to a specially designed, de-mountable sample holder which travels with the sample throughout all measurement and processing steps (for example, gold-coating – see below) and permits replacement of the sample within the spectrometer cryostat with an accuracy estimated to be ±10 μm. The shift due to thermal contraction of the cryostat cold-finger is compensated by a remote-operated z-stage, which can reindex the sample to its original position to within ±2.5 μm accuracy.

To correct for the roughness of the sample surface, we normalized the sample spectrum with a spectrum measured again at the same temperature after evaporating gold on the sample surface. The gold-coating does not change the sample roughness appreciably, being less than 100 nm thick, whereas the roughness observed in an optical microscope is on the order of 10 μm. Although the scattering properties of the gold-coated surface are slightly different from that of the nanotubes, on account of the different refractive indices of the two materials, the correction is a reasonable first-order procedure. Indeed the two factors partially compensate: the rough gold surface is probably a stronger scatterer that the rough nanotube surface, but the gold-coating slightly softens the roughness, diminishing the scattering.

The light-source and spectrometer stability was monitored by measuring a gold reference mirror also

* Corresponding author. Fax: +1-352-392-3591.
E-mail address: tanner@phys.ufl.edu (D.B. Tanner).

1567-1739/01/$ - see front matter
PII: S1567-1739(00)00009-2

located in the cryostat; it showed no significant change during the experiment period. The total experimental error is estimated to be within ±0.5% below 1000 cm^{-1}. We have checked the effect of shifting our reflectance up and down by the possible experimental error of 0.5% on our Kramers–Kronig results; the shift only generates small quantitative effects on the optical conductivity. For the higher frequency region, the reflected light becomes more diffuse due to the roughness of the sample surface, and the error increases to ±2.5% at 5000 cm^{-1}. However, the errors in this higher frequency region did not qualitatively affect the far-infrared conductivity discussed later. We also investigated the temperature dependence of the film dc conductivity by a 4-probe method to compare the dc results with the extrapolated optical conductivity.

Fig. 1 shows the reflectance of the SWNT film measured at about 8 and 300 K. The temperature dependence is quite small, and no vibrational structure is observed even at low temperatures, except for a small kink at 510 cm^{-1}. (In contrast, graphite exhibits [11] an in-plane stretching mode at 1589 cm^{-1}.) The spectra have a Drude-like appearance: the reflectivity monotonically decreases as photon energy increases, with a plasma minimum around 2500 cm^{-1}. Fig. 2 shows the 300 K results for a second film. The data are carried to higher frequencies (25,000 cm^{-1}; 3.1 eV). In the overlap region, the results are qualitatively similar, with the plasma minimum at the same frequency but with a somewhat higher far-infrared reflectance. The difference is attributed to a denser morphology in these samples [12,13]. The reflectance of both materials differs from that of graphite [14], which has its plasma edge at higher frequencies and a strong interband transition around 45 cm^{-1}. The latter dominates in the far-infrared region, causing a reflectance peak around 100 cm^{-1}, and masks the contributions from the free carriers.

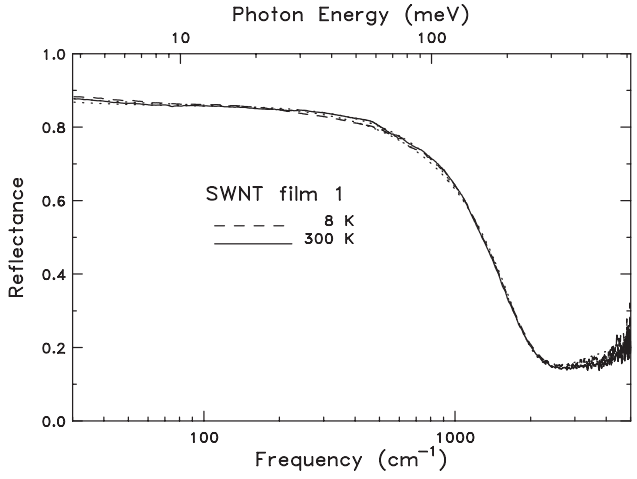

Fig. 1. Reflectance of a SWNT film measured at 8 and 300 K. The dotted lines show the fit to a Drude–Lorentz model (see text).

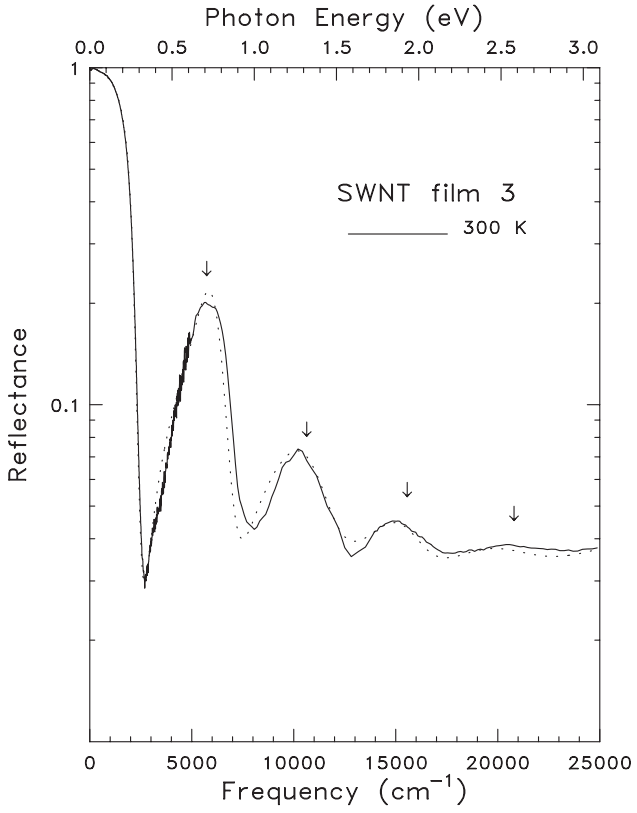

Fig. 2. Reflectance of a second SWNT film measured at 300 K. The dotted lines show the fit to a Drude–Lorentz model (see text).

However, neither SWNT sample is well fit by a Drude response alone. Instead, a Drude–Lorentz model is required, with at least one Lorentz oscillator located at low frequencies (~100 cm^{-1}). The reflectance was fit using the following model dielectric function:

$$\epsilon(\omega) = \epsilon_\infty - \frac{\omega_{\mathrm{pD}}^2}{\omega^2 + \mathrm{i}\omega/\tau_{\mathrm{D}}} + \sum_j \frac{\omega_{\mathrm{p}j}^2}{\omega_j^2 - \omega^2 - \mathrm{i}\omega\gamma_j}, \qquad (1)$$

yielding estimates of the high frequency dielectric constant, ϵ_∞, the Drude plasma frequency, $\omega_{p\mathrm{D}}$, the Drude lifetime τ_{D}, as well as the 'plasma frequency' (oscillator strength), $\omega_{\mathrm{p}j}$, center frequency, ω_j, and damping, γ_j, of each mode. The results for the two samples are shown in Table 1.

The reflectance calculated with the parameters given in Table 1 is shown in both Figs. 1 and 2 as dotted lines. For the data in Fig. 1 a single localized absorption is needed to get good agreement. The localized band has about 33% of the total low energy spectral weight, and is attributed to intrinsic properties of the sample rather than extrinsic features such as impurities [12]. The parameters are almost the same at both temperatures, except that the relaxation rate $1/\tau$ is significantly larger at low temperature. The zero-frequency conductivity

Table 1
Drude–Lorentz parameters from fits to reflectance (all in cm^{-1})

	Center frequency	Oscillator strength	Damping
Sample 1, 300 K			
Drude	–	5200	2000
L1	160	3600	340
L2	6000	7500	3000
Sample 1, 8 K			
Drude	–	5200	2900
L1	170	3800	330
L2	6000	7500	3000
Sample 3, 300 K			
Drude	–	4100	12
L1	70	860	10
L2	5800	5500	1300
L3	10,800	6700	3800
L4	15,700	5000	3800
L5	2100	6100	7200

given by $\sigma_1(0) = \epsilon_0\omega_{pD}^2\tau$ is $\sim$220 $\Omega^{-1}cm^{-1}$ at 300 K and 160 $\Omega^{-1}cm^{-1}$ at 8 K. The non-metallic behavior (decreasing conductivity at low temperatures) is consistent with the semiconducting transport properties of this film [12].

For the sample whose reflectance is shown in Fig. 2, we used four Lorentzians (at locations shown with arrows) to describe the data above the 2500 cm^{-1} plasma minimum. In addition, the far-infrared region was fitted with a Drude (free carrier) term, a low frequency localized absorption, and a broad background absorption extending over 4000 cm^{-1}. The widths of the Drude and far-IR Lorentzian term were quite narrow (12 and 10 cm^{-1}, respectively), consistent with the very high far-IR reflectance. These widths are comparable to what one would estimate for graphite. Recently we have reported that a better fit can be obtained by including a spread of narrow oscillators, up to perhaps eight, in the far-infrared [13].

In Fig. 3 we show the real part of the conductivity (σ_1), obtained by Kramers–Kronig transformation of the reflectance of SWNT film 1 [12]. The dielectric functions from an electron energy-loss (EELS) experiment [15] were used to calculate an extrapolated reflectance to high frequencies; the fitting results of Table 1 were used at low frequencies. The conductivity shows a strong peak at 135 cm^{-1} (17 meV), corresponding to the Lorentzian absorption mentioned above. The temperature dependence is very small. The extrapolated dc conductivity is 200 $\Omega^{-1}cm^{-1}$ at 300 K and 150 Ω^{-1} cm^{-1} at 8 K, in good agreement with what is obtained by the fit to Eq. (1) and in reasonable agreement with the measured dc conductivity. The localized absorption dominates the spectra, despite its smaller weight in the fit above. The contribution of free carriers is not predominant anywhere the measured spectral range on account of their higher damping rate.

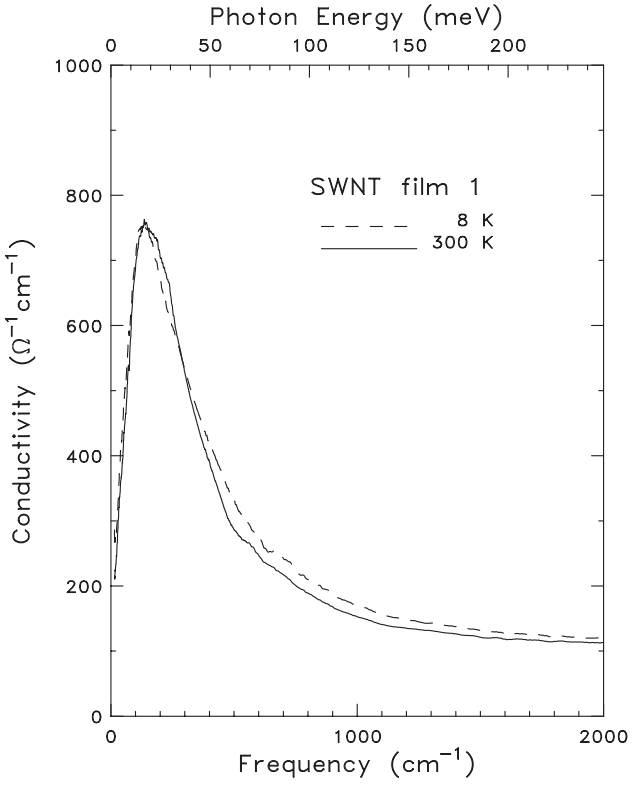

Fig. 3. Real parts of the conductivity ($\sigma_1(\omega)$) of a SWNT film obtained by a Kramers–Kronig analysis of the reflectance.

SWNT electronic structure is specified by a pair of integers (n, m) which represent a coordinate of the wrapping vector in the hexagonal lattice of a single graphite sheet [3]. Hamada et al. [2] used tight-binding calculations to predict that armchair SWNT of $n = m$ are gapless (metallic), whereas zigzag $(n, 0)$ or chiral SWNT ($n \neq m$ and $m \neq 0$) have gaps that vary depending on the wrapping vector. These features were explained by Kane and Mele [7] as follows: most of the SWNT have a primary gap (scaling as $1/R$, where R is the tube radius) about 1 eV, but in one case, $n \equiv m$ (mod 3), this gap nearly vanishes. There remains, however, a very small gap, $\sim$10 meV and scaling as $1/R^2$, induced by the tube curvature; this secondary gap vanishes only in the $n = m$ armchair tubes [7]. In case where these (n, n) SWNT are organized into bundles or ropes, moreover, Delaney et al. [8] argued using an empirical pseudopotential method that the intertube couplings cause a broken symmetry of the tube, inducing a pseudogap at the Fermi level. Either or both of these effects could be responsible for the far-infrared gap-like feature in our spectra.

The modest temperature dependence and the persistence of the gap to room temperature may seem unusual. We note, however, that at room temperature

graphite has an electronic gap-like feature at 45 cm^{-1}, even lower than in our samples: this feature is similarly weakly temperature-dependent [14]. Furthermore, unlike a semiconductor, the density of mobile carriers in our nanotube sample is large even at low temperatures. Moreover, the gap here is caused by symmetry and hence is not as vulnerable to temperature as a CDW or superconducting gap. At higher energies, the data in Fig. 2 correspond to transitions between densities-of-states peaks found in electronic structure calculations [2,3,7,16,17].

Recently, unusual orientation-dependent behaviors were measured in polarized Raman spectroscopy on fibers of aligned SWNT [18,19]. In particular, it was observed that for scattered light analyzed parallel to the incident laser-polarization (VV geometry) all SWNT Raman peaks evidenced a dramatic decrease in intensity as the fiber orientation was rotated from parallel to perpendicular with respect to the incident polarization. This behavior is contrary to expectations based on the assigned symmetry of the associated vibrational modes, which would predict that some lines should decrease more rapidly than others. This orientation dependence in the Raman scattering was ascribed to the known resonance enhancement in the Raman spectra of SWNT [20] and an assumed orientation dependence of the absorption responsible for the resonance. In this contribution we report polarized reflectance and absorption spectra measured on oriented fibers of aligned SWNT, providing direct confirmation of the previously assumed polarization-dependent optical absorption. Such anisotropy in the optical absorption of nanotubes was predicted by Ajiki and Ando [16] and elaborated by Tasaki et al. [17].

Aligned SWNT fibers were generated by a novel method involving the electrophoretic attraction of the nanotubes suspended in dimethylformamide (DMF) to a positively charged 8 μm diameter carbon fiber (CF). The SWNT aggregate about this electrode, forming an extended network of nanotubes attached to the electrode and to each other. Upon slow withdrawal of the CF from the solution, a free-standing fiber of SWNT (attached on one end to the CF) is drawn from the network remaining in the solution [18]. The resulting SWNT fibers have diameters of typically 2–10 μm, lengths up to several centimeters, and moderate alignment of the nanotubes along the fiber axis. The alignment was qualitatively verified by SEM, TEM, selected area electron diffraction and quantified as described below by polarized Raman spectroscopy.

We measured the reflectivity of the free-standing fiber using a Zeiss MPM-800 microscope photometer equipped with polarizer and analyzer over wavelengths of 800–400 nm (1.5–3 eV or 12,000–25,000 cm^{-1}). The measurement aperture in the plane of the sample was 50×50 μm^2. However, the sample underfilled the aperture so the effective area was of order 10×50 μm^2. To measure the polarization parallel and perpendicular to the fiber axis, we kept the polarizer/analyzer fixed and rotated the specimen.

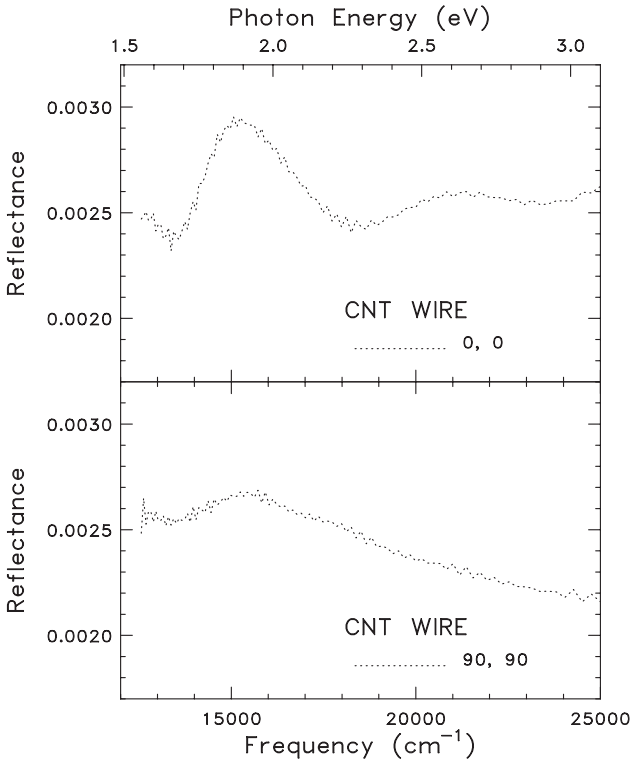

Fig. 4. Polarized reflectivity of a free-standing fiber made up of single-wall carbon nanotubes for electric field parallel (upper panel) and perpendicular (lower panel) to the fiber (and SWNT) axis.

Fig. 4 shows the polarized reflectivity of a free-standing SWNT fiber for electric field parallel (upper panel) and perpendicular (lower panel) to the fiber (and SWNT) axis. Considerable anisotropy is evident. In particular, the bands at 15,300 cm^{-1} (1.9 eV) and 21,000 cm^{-1} (2.6 eV) are strongly polarized in the parallel direction, although some of the more intense 15,300 cm^{-1} feature appears in the perpendicular polarization due to the misaligned SWNT in the fiber. As already mentioned, the curved surface and small area of the fiber gives large systematic errors in the magnitude of the reflected signal; however, we believe that the spectral features are accurately given by these data. Thus, the result that the two absorptions are strongly polarized along the tube axis confirms the interpretation of the polarization-dependence of the Raman spectrum as due to matrix element effects in the resonant enhancement factors.

Acknowledgements

This work was supported in part by the National Science Foundation through DMR-9705108.

References

[1] S. Iijima, Nature (London) 354 (1991) 56.
[2] N. Hamada, S. Sawada, A. Oshiyama, Phys. Rev. Lett. 68 (1992) 1578.
[3] R. Saito et al., Appl. Phys. Lett. 60 (1992) 2204.
[4] S.J. Tans et al., Nature (London) 386 (1997) 474.
[5] E.W. Wong, P.E. Sheehan, C.M. Lieber, Science 277 (1997) 1971.
[6] M.B. Nardelli, B.I. Yakobson, J. Bernhole, Phys. Rev. B 57 (1998) R4277.
[7] C.L. Kane, E.J. Mele, Phys. Rev. Lett. 78 (1997) 1932.
[8] P. Delaney et al., Nature (London) 391 (1998) 466.
[9] A. Thess et al., Science 273 (1996) 483.
[10] A.G. Rinzler et al., Appl. Phys. A 67 (1998) 29.
[11] R.J. Nemanich, G. Lucovsky, S.A. Solin, Solid State Commun. 23 (1977) 117.
[12] A. Ugawa, A.G. Rinzler, D.B. Tanner, Phys. Rev. B 60 (1999) R11305.
[13] A. Ugawa, A.G. Rinzler, D.B. Tanner, Ferroelectrics 249 (2001), to appear.
[14] Y. Sato, J. Phys. Soc. Jpn. 24 (1968) 489; H. Philipp, Phys. Rev. B 16 (1977) 2896.
[15] T. Pichler et al., Phys. Rev. Lett. 80 (1998) 4729.
[16] H. Ajiki, T. Ando, Physica B 201 (1994) 349.
[17] S. Tasaki, K. Maekawa, T. Yambe, Phys. Rev. B 57 (1998) 9301.
[18] H.H. Gommans et al., J. Appl. Phys. 88 (2000) 2509.
[19] R. Haggenmueller et al., Chem. Phys. Lett. (2000), accepted.
[20] A.M. Rao et al., Science 275 (1997) 187.